Correlated oscillations of the magnetic anisotropy energy and orbital moment anisotropy in thin films: The role of quantum well states

L. M. Sandratskii

Max-Planck-Institut für Mikrostrukturphysik, Weinberg 2, D-06120 Halle, Germany

We report the first-principles study of the correlated behavior of the magnetic anisotropy energy (MAE) and orbital moment anisotropy (OMA) as the functions of the thickness N of the Fe film. The work is motivated by recent experimental studies combining photoemission, x-ray magnetic circular dichroism, and magnetic anisotropy measurements. In agreement with experiment, the correlated oscillations of MAE(N) and OMA(N) are obtained that have their origin in the formation of the $3d$ quantum well states (QWS) confined in the films. The main contribution to the oscillation amplitude comes from the surface layer. This is an interesting feature of the phenomenon consisting in the peculiar dependence of the physical quantities on the thickness of the film. We demonstrate that the band structure of the bulk Fe does not reflect adequately the properties of the $3d$ QWS in thin films and, therefore, does not provide the basis for understanding the oscillations of MAE(N) and OMA(N). A detailed point-by-point analysis in the two-dimensional (2D) Brillouin zone (BZ) of the film shows that the contribution of the Γ point, contrary to a rather common expectation, does not play an important role in the formation of the oscillations. Instead, the most important contributions come from a broad region of the 2D BZ distant from the center of the BZ. Combining symmetry arguments and direct calculations we show that orbital moments of the electronic states possess nonzero transverse components orthogonal to the direction of the spin magnetization. The account for this feature is crucial in the point-by-point analysis of the OMA. On the basis of the calculations for noncollinear spin configurations we suggest interpretations of two interesting experimental findings: fast temperature decay of the oscillation amplitude in MAE(N) and unexpectedly strong spin mixing of the initial states of the photoemission process.

PACS number(s): 75.30.Gw, 75.70.Ak, 75.70.Tj

I. INTRODUCTION

An important task of modern physics and technology is the design and fabrication of nanoscale devices with desired properties. For the spintronic devices containing magnetic components one of the crucial characteristics is the magnetic anisotropy (MA). It was first predicted theoretically [1] and soon confirmed experimentally [2] that the quantum confinement of the electronic states in the nano-sized components of the samples leads to the oscillation of the MA as the function of the dimension of the components. This provides a useful tool for tuning the properties of the devices and stimulates the study of the effect.

The nonmonotonic behavior of electronic properties as a function of the monotonically increasing size of the components of the system is not a rare phenomenon. Among the oscillating properties are the interlayer exchange coupling through a nonmagnetic spacer [3–5], photoemission intensity [6,7], magnetoresistance [8], magneto-optical properties [9], and surface reactivity [10]. In the case the quantum well states (QWS) are of predominantly sp-character the periods of the oscillations were related to the features of the Fermi surface of the corresponding bulk material [6,11–13]. On the other hand the leading contribution to the MA comes from the $3d$ electrons experiencing much stronger spin-orbit coupling (SOC) than the free-electron-like sp electrons. Therefore the quantum confinement of the $3d$ states is expected to result in strong influence on the MA. The experimental detection of the $3d$ QWS is much more difficult than that of the QWS formed by the free-electron-like states. [14] As a result the number of the experimental studies devoted to the $3d$ QWS is scarce. The scarceness of the experimental research explains a small

number of the theoretical works dealing with the oscillations of the MAE(N) and OMA(N). As important exceptions we can mention the calculations by Cinal *et al.* performed with the parametric tight-binding method (see, e.g., Refs. [1,15] and references therein) and first-principles studies by Guo [16] and Szunyogh *et al.* [17].

Recently in a series of experimental works [18–22], the presence of large MA oscillations was shown for the Fe films on the Ag substrate. The experiments were mainly performed on the films grown on the vicinal Ag surfaces. The presence of steps on the substrate surface leads to the anisotropy of the in-plane x and y axes of the Fe film absent in the ideally flat films. This in-plane anisotropy is the main focus of the experimental works. The authors treat the oscillation of the MA with the variation of the thickness of the Fe film as an intrinsic property of the films and consider the step density as an additional degree of freedom that can be used to tune the functionality of materials [21,22]. The oscillating behavior was observed also in the photoemission and x-ray magnetic circular dichroism (XMCD) spectra. [22] The XMCD measurements provide very valuable information on the magnitudes of the orbital moments of magnetic atoms. The anisotropy of the orbital moments in $3d$ ferromagnets is known to be related to the MA [23–25] and enables additional insight into formation of MA.

These interesting experimental data, together with the interpretation suggested in the experimental papers, raise a number of important questions. Thus, the authors argue that the origin of the oscillating behavior of the measured quantities can be traced back to the properties of the few electronic states in the band structure of bulk bcc Fe. In earlier works [18,21] the minority-spin Δ_2 state was considered to

be responsible for the oscillations whereas in the most recent work [22] it was the majority-spin Δ_5 state. The fact that different states were suggested in different papers shows that experimental identification of the electronic states responsible for the oscillating properties is not easy and straightforward.

A joint analysis of the measurements of different physical quantities is very advantageous and helps to obtain deeper insight into the physics of the system. This is fully valid for the study by Dabrowski *et al.* [22] where the results of the photoemission, XMCD, and MA measurements are considered. However, analyzing different experiments it is important to take into account the distinction in the nature of the measured quantities. Thus, if the angle-resolved photoemission provides the information about individual electronic states, the magnetic-anisotropy energy (MAE) and orbital-moment anisotropy (OMA) are the integral physical quantities reflecting the summary effect of all occupied electronic states.

The aim of the present paper is a detailed analysis of the formation of the oscillating behavior of the MAE and OMA. The results of this analysis do not support the assumption that oscillating behavior of the quantities can be traced back to the features of a small number of the electronic states at the $\mathbf{k}_{||}=0$ point in the two-dimensional 2D Brillouin zone (BZ). Instead, the broad region of the 2D BZ distant from the center of the zone supplies the main contribution. A deeper insight provided by the layer-resolved analysis of the OMA shows that the leading contribution to the oscillations comes from the surface layer. This is a nontrivial property taking into account that the physical origin of the oscillating behavior is the QWS confined in the film and sensitive to the film thickness [1].

There are a number of further important observations that were pointed out in the experimental papers but could not find an explanation within simplified models of the electronic structure considered in these papers. Thus, the spin-resolved photoemission [22] has clearly shown that the initial electronic states of the photoemission process, anticipated to be relevant for the oscillating properties of MAE, are strongly spin mixed. The authors remark that this does not agree with the suggested physical picture where these states are expected to be of the spin-up type. Another interesting observation is the disappearance of the MAE oscillations at temperatures much below the Curie temperature [18,21]. The authors conclude that the effect cannot be attributed to thermal fluctuations because of the large spin splitting of the QWS. The reference to the exchange splitting of the electronic states as the quantity determining the energy scale in the temperature dependencies of the properties of ferromagnets is a feature of the Stoner theory. However, the Stoner theory is known to fail to describe the thermodynamics of the $3d$ ferromagnets (see, e.g., review [26] and references therein). For instance, the Stoner theory gives the value of the Curie temperature that is one order of magnitude higher than the experimental one. The fundamental physical process neglected by the Stoner theory is the thermal disordering of atomic moments. We show that the disordering of the atomic spins is an important factor able to contribute decisively to the thermal decrease of the amplitude of the oscillations.

The paper is organized as follows. In Sec. II we present a calculational approach including the analysis of the symmetry properties of the orbital moments of the electronic states.

In Sec. III, the results of the calculations are presented and discussed.

II. CALCULATION APPROACH

A. General description

The calculations are performed with the augmented spherical waves (ASW) method generalized to account for spin-orbit coupling (SOC) and noncollinear magnetism [24,26]. Not only the spin moment but also the orbital moment is treated as a three-dimensional vector. The α projection of the orbital moment of the ith atom is obtained as the sum of expectation values of the angular momentum operator $\hat{l}_\alpha$ for occupied electron states:

$$m_{o\alpha}^i = \frac{1}{\Omega_{BZ}} \int_{\Omega_{BZ}} d\mathbf{k} \sum_{\nu,\varepsilon_{\mathbf{k}}^\nu \leqslant E_F} m_{o\alpha}^i(\mathbf{k}\nu) \quad \alpha = x,y,z, \quad (1)$$

$$m_{o\alpha}^i(\mathbf{k}\nu) = \int_{\Omega_i} d\mathbf{r}\, \boldsymbol{\psi}_{\mathbf{k}}^{\nu+}(\mathbf{r})\hat{l}_\alpha \boldsymbol{\psi}_{\mathbf{k}}^\nu(\mathbf{r}), \quad (2)$$

where ν is the band index, the integration in Eq. (1) is carried out over the BZ, Ω_{BZ} is the BZ volume, the integration in Eq. (2) is carried out over the ith atomic sphere, $\psi_{\mathbf{k}}^\nu$ are spinor wave functions normalized in the unit cell, $\varepsilon_{\mathbf{k}}^\nu$ are the energies of the electron states, and E_F is the Fermi energy.

As with many other density functional theory (DFT) methods, the ASW method uses an atomic basis set for the decomposition of the electronic wave functions that employs the spherical harmonics for the description of the angular dependencies. For the projection of the orbital moment on axis η, used in the definition of the spherical harmonics as a polar axis, one obtains a very useful and physically transparent expression,

$$m_{o\eta}^i = \sum_{m\sigma} m\, n_{m\sigma}^i = \sum_{(m>0),\sigma} m\left(n_{m\sigma}^i - n_{(-m)\sigma}^i\right), \quad (3)$$

where $n_{m\sigma}^i$ is the occupation number for the atomic orbital with magnetic quantum number m and spin projection σ. Most commonly the polar axis η is chosen as the z axis of the Cartesian coordinate system. Equation (3) is valid for both the contribution of an individual electronic state ($\mathbf{k}\,\nu$) and the total atomic moment. In the latter case the sum over occupied states must be performed [see Eq. (1)]. If the occupations of the m and $-m$ orbitals are equal the projection of the orbital moment is zero. We will refer to the difference in the occupations of the m and $-m$ orbitals as $\pm m$ polarization. The presence of the SOC in the spin-polarized systems always leads to the $\pm m$ polarization of the electronic states and the formation of the orbital magnetic moments. Large $\pm m$ polarizability of the electronic states by the SOC is an important factor in the formation of the large atomic orbital moments. On the other hand, the $\pm m$ polarization by the SOC is connected with different energy shifts of the $\pm m$ orbitals caused by the SOC. The dependence of these energy shifts on the direction of the spin moments is the physical origin of the MAE. Thus there is a deep connection between MAE, OMA, and $\pm m$ polarizability by the SOC which is the physical basis of the Bruno relation between MAE and OMA [23].

The calculations were performed for the Fe films with the thickness varying from 6 to 24 monolayers (ML). The crystal structure is a slightly tetragonally distorted bcc structure with in-plane lattice parameter $a = 5.46521$ au corresponding to the lattice parameter of Ag used in experiments as substrate. The out-of-plane lattice parameter $c = 5.42351$ au corresponds to the lattice parameter of the bulk bcc Fe. To simulate the vacuum the layers of the empty spheres were included: eight layers for the even number of the Fe layers and seven layers for the odd number of the Fe layers.

The calculations were carried out for two types of collinear spin structures and noncollinear structures. The collinear structure with atomic spin moments parallel to the normal to the film will be referred to as FM0 and the collinear structure with in-plane directions of the moments as the FM90 structure. Some calculations are performed for noncollinear structures of the type presented in the insert in Fig. 7. We will use the notation of the type NC30 for the noncollinear structure with the characteristic noncollinearity angle $\theta = 30°$.

For each film thickness, the self-consistent calculation was performed for the FM0 structure. The electronic potential thus obtained was used to calculate the band energies and orbital moments of the electronic states for both FM0 and FM90 structures. The calculated quantities were used to evaluate the values of the MAE and OMA. In the calculation of the anisotropy we subtracted from the quantity for the FM0 structure the quantity for the FM90 structure. The MAE per unit cell is calculated as

$$\text{MAE} = E(\text{FM0}) - \text{E}(\text{FM90}), \tag{4}$$

where E is the band energy of the system given by the expression,

$$E = \frac{1}{\Omega_{\text{BZ}}} \int_{\Omega_{\text{BZ}}} d\mathbf{k} \sum_{\nu, \varepsilon_{\mathbf{k}}^{\nu} \leqslant E_F} \varepsilon_{\mathbf{k}}^{\nu}. \tag{5}$$

According to definition (4), for the negative value of the MAE the easy axis is parallel to the normal to the film. For the noncollinear structures the comparison is performed between configurations with net magnetization parallel to the normal to the film and the corresponding configuration with in-plane net magnetization. The sufficiently dense mesh of the $\mathbf{k}$ points was used. In-plane square 2D BZ contained at least 900 $\mathbf{k}$ points (30×30 mesh) that corresponds to $\sim$54 000 points in the BZ of the bulk bcc lattice.

An important part of the study is the point-by-point analysis of the contributions to the MAE and OMA aiming to reveal the regions of the 2D BZ governing the formation of the anisotropy properties. To perform the point-by-point comparison of the FM0 and FM90 structures we proceeded as follows. A uniform $\mathbf{k}$ mesh of 900 $\mathbf{k}_{\parallel}$ points is selected in the 2D BZ of the films. The calculated energy states at all 900 $\mathbf{k}_{\parallel}$ points are filled globally starting from the lowest energy state. The total number of electrons is known and corresponds to eight valence electrons per Fe atom. If the highest occupied state is degenerate the number of remaining electrons is equally divided between all degenerate states. The energy and orbital-moment contributions of a given $\mathbf{k}_{\parallel}$ point are calculated by summing up the contributions of all occupied states at this $\mathbf{k}_{\parallel}$ with account for the occupation numbers of the states.

The components of the $\mathbf{k}$ vectors are given in units of $\frac{2\pi}{a}$.

B. Symmetry analysis

In this subsection we consider symmetry properties of the orbital moments of the electronic states. The result of this consideration is important for the analysis of the contributions to OMA of different $\mathbf{k}_{\parallel}$.

In the evaluation of the OMA between FM0 and FM90 structures it seems natural to use the expression,

$$\text{OMA} = m_{oz}(\text{FM0}) - m_{ox}(\text{FM90}). \tag{6}$$

However, in the analysis of the contributions of individual $\mathbf{k}_{\parallel}$ points the application of Eq. (6) can lead to misleading results. Close correlation between MAE and OMA suggested by Bruno [23] assumes that both quantities vanish in the absence of the SOC. However, as we will show, the quantity,

$$\text{OMA}^i(\mathbf{k}_{\parallel}) = m_{oz}^i(\text{FM0}, \mathbf{k}_{\parallel}) - m_{ox}^i(\text{FM90}, \mathbf{k}_{\parallel}), \tag{7}$$

corresponding to a point $\mathbf{k}_{\parallel}$ and atom i is, in general, not zero in the absence of the SOC. The symmetry analysis performed below shows that in the FM0 spin structure the x component of the orbital moment of the electron states is not zero. Direct calculations confirm this conclusion and demonstrate that this component can be very large depending on the $\mathbf{k}_{\parallel}$ point. The origin of this contribution to the orbital moment of the electronic state is not in the SOC but in the complex nature of the Bloch states. To obtain the OMA contribution of a $\mathbf{k}_{\parallel}$ point that is caused by the SOC and correlates with the MAE contribution of this point the expression (7) must be modified [see Eq. (8) below].

In the quantum mechanics, the symmetry group consists of the operations that commute with the Hamiltonian of the problem. If the SOC is not taken into account the symmetry is described by the so-called spin-space groups that allow separate transformation of the spin and space variables [26]. In the absence of the SOC, the FM0 and FM90 structures are equivalent, their electronic states are characterized by certain spin projections and the transformation properties of the orbital parts of the wave functions are described by the irreducible representations of the space group of the orbital transformations. This space group is the same for FM0 and FM90 structures and is routinely used to characterize electronic states in nonrelativistic calculations.

If the SOC is taken into account, only the operations transforming in the same way both spin and orbital variables enter the symmetry group. In this case the symmetries of the FM0 and FM90 structures are essentially different. In Table I we collect the point symmetry operations of the FM0 and FM90 structures in the case of the SOC taken into account. In magnetic systems the pure time reversal is not a symmetry operation. It, however, enters the symmetry group in combination with space transformations. The third and fourth columns give the results of the transformation of $\mathbf{k}_{\parallel}$ and orbital magnetic moment of an electronic state under the action of the symmetry operation. Since $\mathbf{k}_{\parallel}$ is a polar vector and magnetic moment is an axial vector, they are transformed differently by the space inversion, reflections in the planes, and improper rotations.

TABLE I. Symmetry operations of the FM0 and FM90 structures. First column, number of the operation. Second column, symbol of the operation. E is the unity operation; $C_{n\alpha}$ are proper rotations by angle $2\pi/n$ about the α axis; $\alpha = x,y,z$ correspond to the x,y,z axes, $\alpha = a$ corresponds to the $y = x$ axis in the $z = 0$ plane, $\alpha = b$ corresponds to the $y = -x$ axis in the $z = 0$ plane; $S_{4z}^{\pm}$ are improper rotations about the z axis by angle $\frac{\pi}{2}$; σ_{β} is the reflection in the β plane, $\beta = x,y,z$ correspond to the $x = 0$, $y = 0$, $z = 0$ planes, $\beta = a$ corresponds to the $y = -x$ plane, $\beta = b$ corresponds to the $y = x$ plane, T is the time reversal operation. Third column, the result of the action of the operation on vector (k_x,k_y). Fourth column, the result of the action of the operation on vector (m_x,m_y,m_z). Fifth column, i stands for the case that each layer is transformed into itself; $N - i + 1$ stands if the operation transforms layer i into layer $N - i + 1$.

No.	OP	$\mathbf{k}$	$\mathbf{m}$	Layer
		FM0		
1	E	(k_x,k_y)	(m_x,m_y,m_z)	i
2	C_{2z}	$(-k_x,-k_y)$	$(-m_x,-m_y,m_z)$	i
3	C_{4z}^{-}	$(k_y,-k_x)$	$(m_y,-m_x,m_z)$	i
4	C_{4z}^{+}	$(-k_y,k_x)$	$(-m_y,m_x,m_z)$	i
5	I	$(-k_x,-k_y)$	(m_x,m_y,m_z)	$N - i + 1$
6	σ_z	(k_x,k_y)	$(-m_x,-m_y,m_z)$	$N - i + 1$
7	S_{4z}^{+}	$(-k_y,k_x)$	$(m_y,-m_x,m_z)$	$N - i + 1$
8	S_{4z}^{-}	$(k_y,-k_x)$	$(-m_y,m_x,m_z)$	$N - i + 1$
9	TC_{2x}	$(-k_x,k_y)$	$(-m_x,m_y,m_z)$	$N - i + 1$
10	TC_{2y}	$(k_x,-k_y)$	$(m_x,-m_y,m_z)$	$N - i + 1$
11	TC_{2b}	(k_y,k_x)	(m_y,m_x,m_z)	$N - i + 1$
12	TC_{2a}	$(-k_y,-k_x)$	$(-m_y,-m_x,m_z)$	$N - i + 1$
13	$T\sigma_x$	$(k_x,-k_y)$	$(-m_x,m_y,m_z)$	i
14	$T\sigma_y$	$(-k_x,k_y)$	$(m_x,-m_y,m_z)$	i
15	$T\sigma_b$	$(-k_y,-k_x)$	(m_y,m_x,m_z)	i
16	$T\sigma_a$	(k_y,k_x)	$(-m_y,-m_x,m_z)$	i
		FM90		
1	E	(k_x,k_y)	(m_x,m_y,m_z)	i
2	C_{2x}	$(k_x,-k_y)$	$(m_x,-m_y,-m_z)$	$N - i + 1$
3	I	$(-k_x,-k_y)$	(m_x,m_y,m_z)	$N - i + 1$
4	σ_x	$(-k_x,k_y)$	$(m_x,-m_y,-m_z)$	i
5	TC_{2y}	$(k_x,-k_y)$	$(m_x,-m_y,m_z)$	$N - i + 1$
6	TC_{2z}	(k_x,k_y)	$(m_x,m_y,-m_z)$	i
7	$T\sigma_y$	$(-k_x,k_y)$	$(m_x,-m_y,m_z)$	i
8	$T\sigma_z$	$(-k_x,-k_y)$	$(m_x,m_y,-m_z)$	$N - i + 1$

For a general $\mathbf{k}_{\|}$ point with arbitrary values of coordinates k_x and k_y, all points obtained by the action of the symmetry operations are different and form the so-called star of vector $\mathbf{k}_{\|}$ containing eight vectors for the FM0 structure and four vectors for the FM90 structure (Fig. 1). Half of the symmetry operations leave all atoms in the same layer. The other half of the operations transform layers i and $N - i + 1$ into each other.

As follows from Table I, for a general $\mathbf{k}_{\|}$ of the FM0 structure the z components of the atomic orbital moments for all eight symmetry related electronic states are equal to each other in layers i and $N - i + 1$. The x and y components of the orbital moments are also symmetry related but in a more complex way (Fig. 1). Thus, the knowledge of the atomic orbital moment in layer i for one state of the star uniquely determines the orbital moments in layers i and $N - i + 1$ for all eight vectors of the star. However, the symmetry
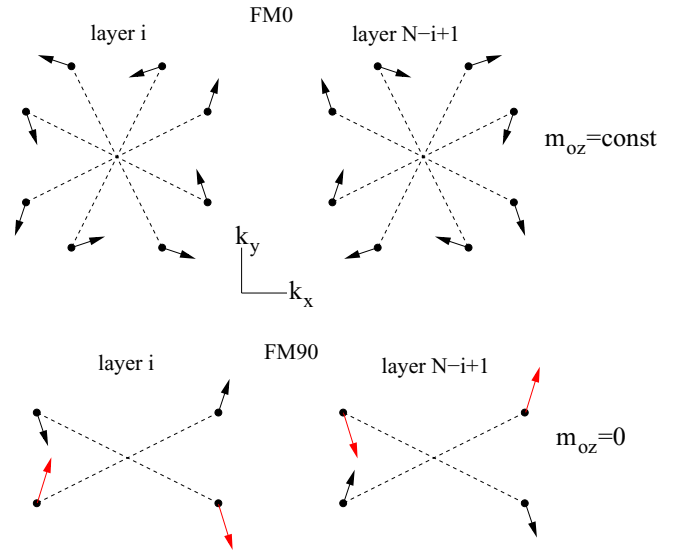

FIG. 1. (Color online) Symmetry properties of the orbital moments of the electronic states. Black solid circles show equivalent $\mathbf{k}_{\|}$ points forming the star of the corresponding wave vectors. The star contains eight vectors for the FM0 structure and four vectors for the FM90 structure. The arrows show the in-plane components of the orbital moments of the electronic states for the pairs of the symmetry related layers: ith and $(N + 1 - i)$th. In the FM0 structure all in-plane components are nonzero and symmetry connected. In the FM90 structure for each of the states the orbital moments in ith and $(N + 1 - i)$th layers are different and not symmetry connected. There are, however, symmetry relations between orbital moments of different states. Symmetry-connected orbital moments are shown by the same color (red or black). Different colors correspond to the moments that are not connected by a symmetry relation.

does not impose restrictions on the quantitative values of the components of the atomic orbital moments of the individual $\mathbf{k}_{\|}$ states. In particular, there is no symmetry reason to expect that the x components of the atomic orbital moments are zero for the FM0 structure.

In the FM90 structure, the z component of the atomic orbital moments is zero, by symmetry, for all states and all layers. For the in-plane components we obtain an interesting property that for each of the states the contributions into the ith and $(N - i + 1)$th layers are different (different color arrows in Fig. 1). There is, however, a peculiar symmetry property that the in-plane components of the states in the ith layer are symmetry related to the in-plane components of other states in the $(N - i + 1)$th layer.

The first-principles calculations confirm that the in-plane components of the atomic orbital moments for the FM0 structure are nonzero. As an example, we show in Fig. 2 the components of the orbital moments for atoms of the surface layer calculated for the interval of $\mathbf{k}_{\|}$ points with constant $k_x = 0.5$ and k_y varying from -0.5 to 0.5. We see that in the case of FM0 structure the x component of the orbital moment is large. In agreement with the symmetry analysis it is odd with respect to the change of the sign of k_y in contrast to the z component that is even with respect to the sign change of k_y. As mentioned above, this large x component of the orbital moment has its origin not in the SOC but in the complex
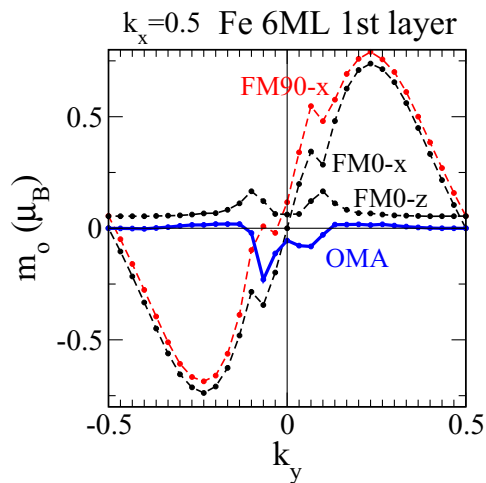
FIG. 2. (Color online) The components of the orbital moments for atoms of the first layer of the 6-ML-thick film. The results are presented for the interval $\mathbf{k}_{||} = (0.5, k_y)$ where k_y varies from -0.5 to 0.5. Curves marked with FM0-x and FM0-z show the x and z projections of the orbital moment in the case of the FM0 structure. FM90-x corresponds to the x projection in the case of the FM90 structure. OMA is calculated as given by Eq. (8).

nature of the Bloch functions. The large SOC-independent contribution to the x component of the orbital moment is present for both FM0 and FM90 structures. As a result, the x component of the orbital moment in the FM90 structure is also large and unsymmetric with respect to the sign reversal of k_y. The contribution to the OMA of the atom of layer i coming from the point $\mathbf{k}_{||}$ calculated as

$$OMA^i(\mathbf{k}_{||})$$
$$= m_{oz}^i(FM0, \mathbf{k}_{||}) - \left[m_{ox}^i(FM90, \mathbf{k}_{||}) - m_{ox}^i(FM0, \mathbf{k}_{||}) \right], \quad (8)$$

vanishes with vanishing SOC and is a useful quantity for the $\mathbf{k}_{||}$-resolved analysis of the formation of the SOC-caused OMA and its relation to MAE. On the other hand, the neglect of large $m_{ox}^i(FM0, \mathbf{k}_{||})$ in Eq. (8) gives the quantity that does not vanish with vanishing SOC and cannot be related to the contributions to the MAE.

If some of the symmetry operations leave vector $\mathbf{k}_{||}$ invariant (so-called high-symmetry $\mathbf{k}_{||}$ points), the transformation properties impose restrictions on the value of the orbital moment at this point. For example, all symmetry operations leave Γ point $(0,0)$ invariant and the restrictions on the atomic orbital moments of the states at Γ result, in the case of FM0, in $m_{ox} = m_{oy} = 0$ for all layers.

III. RESULTS AND DISCUSSION

A. Integrated quantities

We begin with the discussion of the integrated quantities. There are two contributions to the MAE. One has its origin in the influence of the SOC on the electronic states and the other is due to the magneto-static dipole-dipole interaction of the atomic magnetic moments [27]. The N dependence of both contributions is presented in Figs. 3(a) and 3(b). The electronic contribution [Fig. 3(b)] is negative for all N showing
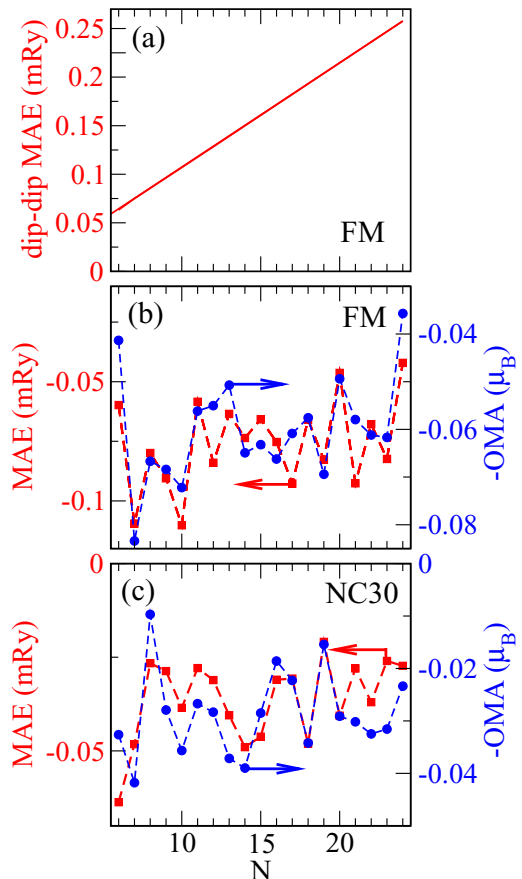

FIG. 3. (Color online) Anisotropies as the function of the film thickness. (a) MAE due to the dipole-dipole interaction; (b) MAE and $-$OMA due to the SOC for the ferromagnetic structure; (c) MAE and $-$OMA due to the SOC for the noncollinear structure with characteristic noncollinearity angle $\theta = 30°$. The anisotropy energies are calculated per unit cell.

that the SOC tends to make the out-of-plane direction of the magnetization energetically preferable. This contribution competes with the contribution due to the magneto-static interaction. In agreement with previous studies of the thin films [16,17] the dipole-dipole MAE(N) is a monotonic function of the film thickness [Fig. 3(a)]. As a result of the competition of the two contributions, the thinnest films have an out-of-plane easy axis. With increasing thickness there is a reorientation transition to the state with an in-plane easy axis. This property is in agreement with the experiment where the reorientation transition for the Fe films was indeed detected [28,29]. The oscillating behavior as the function of N is obtained only for the SOC-caused contribution to the MAE [Fig. 3(b)]. In the following we will consider only the electronic contribution.

There is clear correlation in the features of the MAE and OMA N dependencies: The minima and maxima of MAE(N) correspond to the minima and maxima of $-$OMA(N) [Fig. 3(b)]. Such type of correlation is expected for the ferromagnetic transition metals where the main contribution to the MAE and OMA comes from the spin-down states [23,24]. This is true in the case of Fe where the spin-up 3d states are occupied and contribute only weakly to the anisotropies
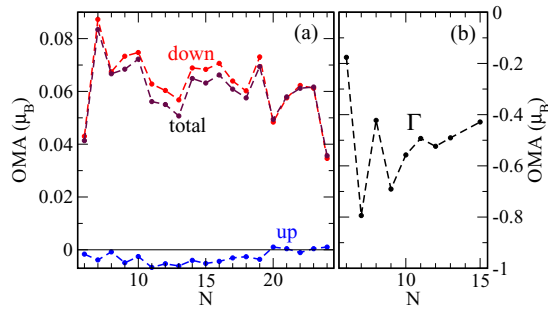
FIG. 4. (Color online) (a) Spin-resolved OMA as the function of the film thickness. (b) The contribution of the Γ point to the OMA(N).

whereas spin-down states are partially occupied and supply the leading contribution. Indeed Fig. 4(a) shows that the contribution of the spin-down states to the OMA is decisive.

The layer-resolved analysis of the OMA shows that the contribution of the surface layers is much larger than the contribution of the rest of the film [Fig. 5(a)]. Remarkably, not only an average OMA value but also the OMA oscillations are strong in the surface-layer contribution and, to a large extent, determine the oscillations of the total OMA. As mentioned in the introduction, this is an interesting property taking into account that for a pure surface effect a strong dependence on the film thickness is not expected. Instead, the oscillations are anticipated to be a consequence of the properties of the QWS that spread over the whole film and, therefore, depend on the film thickness.

To get a deeper insight into interplay of the SOC and QWS we performed two model calculations. In the first calculation, the SOC was switched on in all layers excluding the surface ones. In the second calculation, on the opposite, the SOC was taken into account only in the surface layers. If the surface SOC is switched off, both MAE and OMA of the

FIG. 5. (Color online) (a) Layer-resolved contributions to OMA(N). Numbers enumerate different layers. First layer is the surface layer. (b) Total OMA(N) is calculated with full SOC (full), with the SOC only in the surface layers (surf), and with the SOC only in the inner layers (inner). (c) The surface layer contribution to OMA(N) for three different treatments of the SOC. (d) Total MAE(N) for three different treatments of the SOC.

film drop strongly [Figs. 5(b) and 5(d)]. Simultaneously, the MAE changes sign for all thicknesses demonstrating that pronounced trend to the out-of-plane MAE is the property governed by the surface SOC. In addition, OMA changes sign for all thicknesses besides $N = 7$ and $N = 10$ demonstrating again the correlation between the properties of the two quantities. The layer-resolved OMA data show that, despite the absence of the SOC in the surface layer, the value of the OMA contribution of this layer is comparable with the contributions of the second and third layers (not shown). Remarkably, the surface contribution still oscillates strongly. This clearly shows that there is strong hybridization between the $3d$ orbitals of the surface and inner atoms. Through this hybridization the $\pm m$ polarization of the inner atoms induced by the SOC is transferred to the surface layer.

In the second model calculation with only surface SOC taken into account, MAE(N) and OMA(N) do not change dramatically compared with full-SOC calculation [Figs. 5(b) and 5(d)]. Thus, the values and the signs of the MAE and OMA are mainly determined by the SOC in the surface layer. However, if we focus on the oscillations in the N dependencies of the quantities we notice that they remain rather strong in both model calculations. It is also seen that despite the change of the sign of the MAE(N) and OMA(N) in the calculation with the inner SOC only, the oscillations do not follow this trend: Minima and maxima of the dependencies calculated with full SOC and with only inner SOC are in close correlation. This is especially well seen in the OMA(N). The local minima and maxima coincide for film thicknesses of $N = 6,7,10,13,14,15,18,20,24$ [Figs. 5(b) and 5(d)]. These joint features demonstrate that behind the oscillations there are the properties of the electronic structure of a general nature. This is the QWS due to the quantum confinement. The formation of the QWS is not a relativistic effect. However, the QWS are differently modified by the SOC depending on the orientation of the spin moments with respect to the atomic structure that leads to the anisotropy phenomena.

We remark that our calculations did not give the decay of the amplitude of the oscillations with increasing thickness of the film. In this respect we agree with Szunyogh *et al.* who found nondecaying MAE oscillations in Co films up to the thickness of 40 atomic layers (see Fig. 1 of Ref. [17]). In particular, there is the contribution to the oscillations because of the difference of the QWS in the films with even and odd numbers of layers.
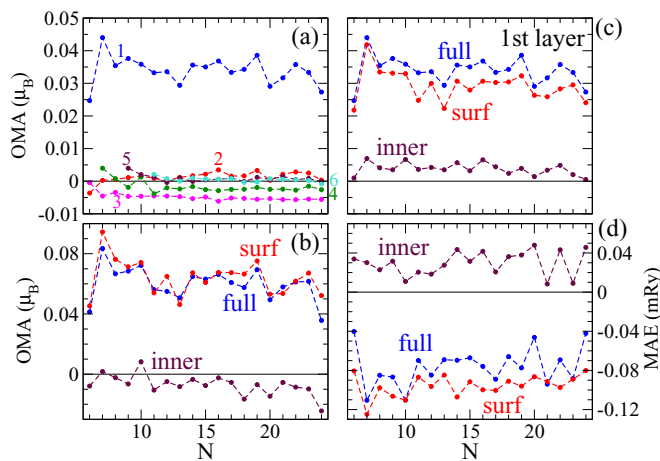
B. QWS and oscillating behavior of physical quantities

It is useful, before going to the consideration of the $\mathbf{k}_{||}$-resolved contributions to MAE and OMA, to briefly discuss the physical origin of the relation between QWS and the oscillation of the physical quantities as the function of the thickness of the nano-sized components of the system. There is an important difference between free-electron-like QWS formed by the sp-electron states and the QWS formed by the $3d$ electron states. The physics of the free-electron QWS can be captured by the consideration of the rectangular quantum wells neglecting the atomic structure of the system. Such QWS can be presented, at each $\mathbf{k}_{||}$, in the form of the linear combinations of the plane waves characterized by certain quantized values of $k_\perp$ where $k_\perp$ is the component of the

wave vector orthogonal to the surface of the film. This justifies the use of the electronic bands and Fermi surface of the corresponding three-dimensional (3D) bulk system in the analysis of the properties of the films.

For the treatment of the confined $3d$ states the consideration of the atomic structure is crucial. In particular, the different atomic environment of the atoms of the surface and inner layers makes the atoms of different layers inequivalent. This inequivalence is reflected in the properties of the electronic states confined in the film. In Fig. 8, we show, as an illustration, the distribution of the $3d$ charge over layers of the 12-layers-thick film for three, close to the Fermi energy, states at a general point $\mathbf{k}_{||} = (0.1, 0.2333)$. In all cases there is large contribution of the surface layers and oscillating contributions of the inner layers. In details, the shapes of the states are very different and cannot be described by a simple general rule.

Another important aspect is the difference between films with odd and even numbers of layers. The atomic positions of both types of films are symmetric with respect to the reflection in the $z = 0$ plane at the middle of the film. For the films with an odd number of layers $N = 2m + 1$ the symmetry plane goes through the mth atomic layer whereas for the films with an even number of layers $N = 2m$ the symmetry plane lies between the mth and $(m + 1)$th atomic layers. Since the symmetry influences the shape of the QWS with respect to the symmetry plane, the situations for the films with even and odd numbers of layers are different. This difference results in oscillating behavior with a period of two atomic layers [17].

In strong contrast to the 3D periodic solids there is considerable charge transfer between atoms of different layers of the films and to the vacuum region presented in our calculations by the empty spheres. In Fig. 6, we show the charge of the Fe atomic spheres belonging to different layers for the films with $N = 8$ and $N = 24$ calculated as $q_n = (n_n^{el} - Z_n)$ where n_n^{el}
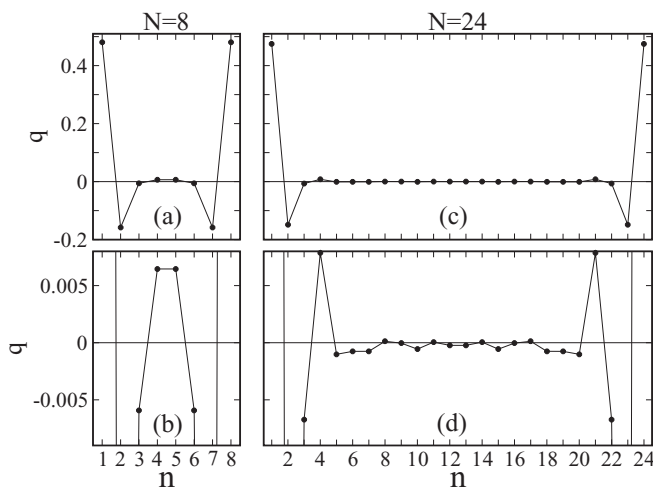

FIG. 6. Deviation of the Fe atomic spheres of different layers from charge neutrality for the films with thicknesses $N=8$ [(a) and (b)] and $N=24$ [(c) and (d)]. The scale of the ordinate axis in (b) and (d) is changed to zoom in the charge properties of the inner atoms. The calculations were performed for the FM0 structure with the SOC included. The fine details of the charge distribution depend on the direction of the atomic moments.
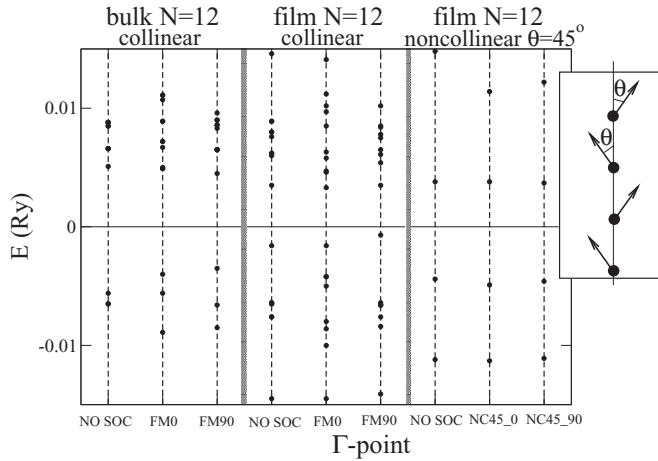
is the number of electrons in the nth atomic sphere and Z_n is the corresponding nuclear charge. The atomic spheres of the surface and first subsurface layers are very strongly charged [Figs. 6(a) and 6(c)]. The charges of the deeper layers are much smaller. However, these charges are also of importance for the small anisotropy quantities. The inequivalence of the layers is a very important factor that makes questionable the possibility of describing the $3d$ QWS of the films in terms of the states of the 3D periodic crystal.

In a 3D periodic crystal the energy bands are continuous functions of the crystal momentum $\mathbf{k}$ varying in the 3D BZ. The number of the $3d$ states at each $\mathbf{k}$ point is the same and is determined by the number of the $3d$ atoms in the unit cell of the crystal. With choosing an increased super cell the number of the atoms in the unit cell and, therefore, the number of the $3d$ states at each $\mathbf{k}$ point increase while the volume of the BZ decreases. Since this downfolding procedure does not change the electronic states they still can be characterized by the Bloch vectors lying outside the decreased BZ. The choice of a bigger unit cell does not disturb either the equivalence of the atoms or the 3D character of the energy spectrum in the reciprocal space.

In the case of a film the situation is different. Here the periodicity and the BZ are two-dimensional. The number of the $3d$ states at a given $\mathbf{k}_{||}$ is again proportional to the number of the $3d$ atoms in the unit cell that corresponds now to the number of the atomic layers in the film. Increased number of the layers leads to increased number of the states and, as a result, to decreased energy distance between them. In contrast to the downfolded states of the 3D periodic bulk, the film states at a given $\mathbf{k}_{||}$ of the 2D BZ cannot be characterized by any further Bloch momentum and unfolding of the states outside the 2D BZ is not possible. The monotonically increasing number of the 3d states with increasing N leads to nonmonotonic variation of the positions of the states with respect to the Fermi level. Since these positions are decisive for many electronic properties the increase of N leads to the nonmonotonic $\mathbf{k}_{||}$ contributions to the N dependencies of the physical properties.

To illustrate the difference of the electronic structures of the film and bulk systems we present in Fig. 7 the electronic states at the Γ point of the reciprocal space calculated for different cases. The comparison of the left and middle panels shows clearly the strong difference of the electronic spectra of the bulk and film as well as the difference in the response of the spectrum to the SOC for the FM0 and FM90 structures.

Since at each individual $\mathbf{k}_{||}$, the energies of the electronic states and, therefore, their positions with respect to the Fermi level are different, the contributions to the N dependence of the electronic properties vary from point to point. It is rather common to assume that the decisive contribution to the nonmonotonic behavior of the electronic properties comes from the Γ point ($\mathbf{k}_{||}=0$) of the 2D BZ. This assumption is not, however, generally valid and, as is shown below, for the properties of MAE and OMA of the thin films does not have solid basis.

Summarizing this section we can formulate a number of conclusions. First, by choosing the proper size of the super cell of the 3D bulk crystal we can get an equal number of the $3d$ states at each $\mathbf{k}$ point of the reciprocal space for both bulk and N-layers-thick film. However, for the bulk crystal

FIG. 7. The electronic states at the Γ point calculated for different cases. (Left panel) The electronic states of the bulk Fe calculated with the super cell containing 12 atoms. (Middle panel) The states of the film with $N = 12$. (Right panel) The states of the noncollinear structure of the $N = 12$ film with angle $\theta = 45°$. Insert gives a schematic picture of the directions of the atomic spin moments of different layers in the noncollinear structure characterized by angle θ. In each panel, the states are calculated in three different ways: without SOC, with SOC, and the direction of the net moment parallel to the normal to the film, and with SOC and the direction of the net moment parallel to the plane of the film.

the procedure of choosing different supercells is a purely mathematical construction providing equivalent descriptions of the same physical object whereas the films of different thicknesses are truly different physical systems. Second, although the $3d$ states are characterized by a discrete set of energies at each **k** point in both bulk and film, in the case of bulk for each $\mathbf{k}_{\parallel}$ there is an infinite number of **k** points with different $k_{\perp}$ values. The summation over $k_{\perp}$ leads to a strong averaging of the contributions of the individual **k** points. In the film the effect of averaging over continuous $k_{\perp}$ is absent. Third, one can attempt to describe the energy spectrum of the film at a given $\mathbf{k}_{\parallel}$ by the downfolded bulk spectrum at the same **k** point. This procedure does not, however, have a solid basis because of strong inequivalence of layers in thin films (see, e.g., Fig. 8). The performance of the first-principles calculations within the framework of the density functional theory for the films of different thicknesses is essential. Fourth, there is difference between QWS in the films with even and odd numbers of layers.

C. Detailed analysis of selected $\mathbf{k}_{\parallel}$ points

In the next section, we will perform systematic analysis of the $\mathbf{k}_{\parallel}$-resolved contributions to the MAE and OMA over the whole 2D BZ. It is, however, instructive to start with few selected $\mathbf{k}_{\parallel}$ points and perform a detailed analysis of the MAE and OMA contributions of these points as a function of the number of occupied states. The character of the dependencies allows us to gain insight into the way the change of the position of the Fermi level leads to a nonmonotonic variation of the physical quantities. As follows from Table I, for the $\mathbf{k}_{\parallel}$ points
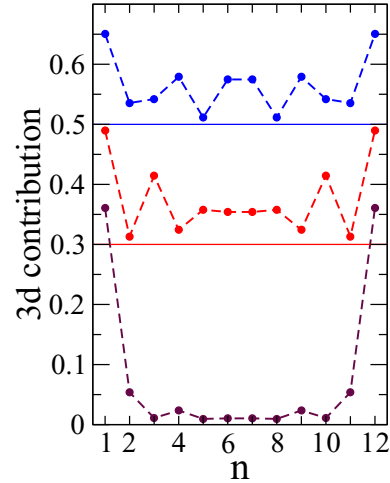

FIG. 8. (Color online) The $3d$ charge distribution over layers of the 12-layers-thick film for three, close to the Fermi energy, states at a general point $\mathbf{k}_{\parallel} = (0.1, 0.2333)$. To improve visual comprehension the red curve is shifted by 0.3 and the blue curve by 0.5.

considered in this section $m_{ox}^{i}(\text{FM0}) = 0$ and expression (7) for OMA can be used instead of (8).

We begin with the consideration of the Γ point. In Figs. 9(a) and 9(d) we present the OM as a function of the number of the occupied states for the films of two different thicknesses, $N = 8$ and $N = 24$. The most clear oscillating behavior is obtained for the FM0 structure. Typically, these oscillations are formed as follows. First, with an increasing number of electrons the absolute value of the OM increases steeply. After the occupation of a few further states the absolute value of the OM decreases again to the magnitude close to that before the steep increase. As a result, the sequence of sharp peaks is formed. These peaks can be associated with the filling of the $3d$ QWS at the Γ point. In the absence of the SOC the orbitals with opposite values of the magnetic quantum number m are equally occupied and the orbital moment is zero [Eq. (3)]. For the spin-up states the on-site SOC moves negative-m orbitals to lower energies and positive-m orbitals to higher energies. Therefore, the states contributing to the negative orbital moment are occupied first. The occupation of higher-energy levels fills the states with predominantly positive m compensating the contribution of the lower levels. Thus clearly resolved peaks are formed. For the spin-down states the character of the $\pm m$ polarization is opposite and the peaks are formed in the positive direction. For the FM90 structure, the nonmonotonic oscillating behavior is also present but much less pronounced.

The oscillating behavior of the FM0 orbital moment leads to strong oscillation of the OMA [Figs. 9(b) and 9(e)]. The MAE [Figs. 9(c) and 9(f)] also show pronounced oscillating behavior. There is strong correlation between the features of the OMA and MAE dependencies. The negative peaks of the MAE in the region of the lower occupation of the electron states correspond to the negative peaks of the OMA coming from the spin-up states whereas the negative MAE peaks at the larger occupation correspond to the positive peaks of the OMA coming from the spin-down states. Thus the change of the sign in the relation between OMA and MAE, depending
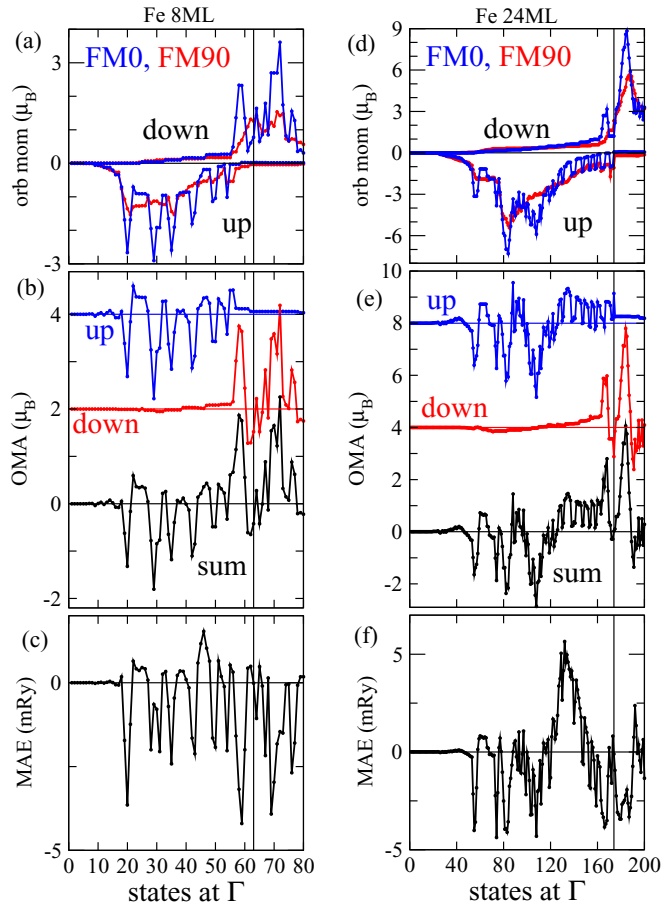
FIG. 9. (Color online) Orbital moment [(a) and (d)], OMA [(b) and (e)], and MAE [(c) and (f)] at the Γ point as the functions of the number of occupied states. Panels (a)–(c) are for 8-ML-thick film, (d) and (e) are for 24-ML-thick film. (a) and (d) Spin-resolved contributions to the orbital moment are shown for FM0 (blue curves) and FM90 (red curves) structures. (b) and (e) Spin-resolved contributions to MAE and total MAE are presented. For convenience the spin-resolved curves are shifted along the ordinate axis by multiples of 2 (b) and 4 (e). The vertical straight lines in the panels show the position of the Fermi level.

FIG. 10. (Color online) Similar to Fig. 9 but for the center of the ΓM interval $\mathbf{k}_{||} = (0.25,0)$ and point M $\mathbf{k}_{||} = (0.5,0)$ of the 8-ML-thick film.

on the spin projection of the states, is clearly observed. The number of the oscillations increases with increasing thickness of the film reflecting the increased number of the QWS as discussed in Sec. III B. Qualitatively, the cases of $N = 8$ and $N = 24$ are similar.

Also for other $\mathbf{k}_{||}$ points (Fig. 10) the nonmonotonic behavior of the quantities is present. However, the dependencies are strongly different for different points. The number of the peaks is less than for the Γ point and the peaks are, on average, less pronounced. The reason for differently pronounced oscillation patterns for different $\mathbf{k}_{||}$ points lays in different symmetry properties of the electronic states. The states of the highest symmetry are at the Γ point of the FM0 structure. In this case there is the largest number of the irreducible representations and the states belonging to different irreducible representations do not interact. Therefore the SOC involves a smaller number of states to $\pm m$ redistribution. As a result, the $\pm m$ redistribution between states and, therefore,
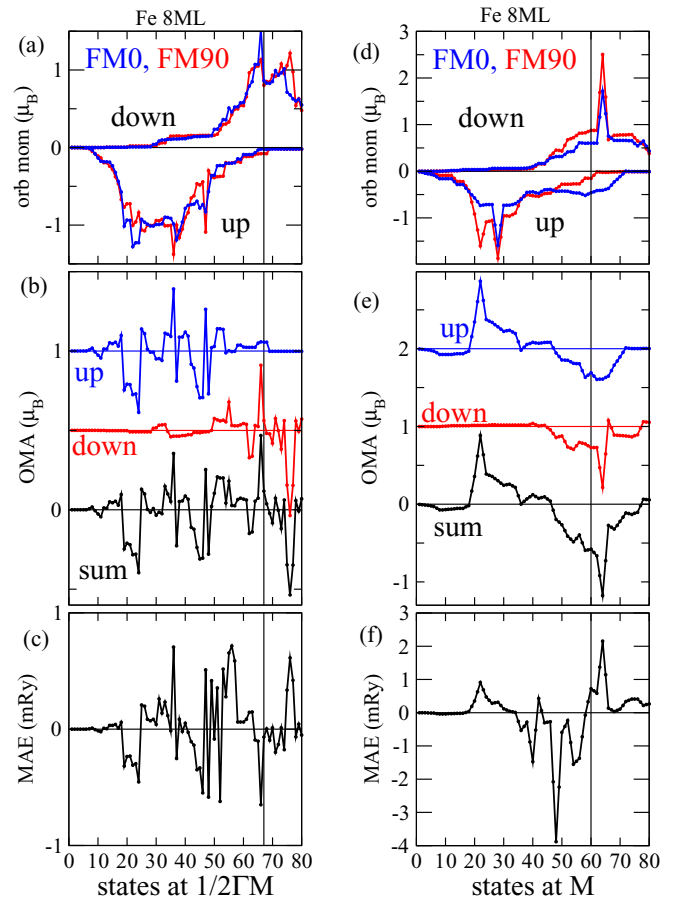
their $\pm m$ polarization are more pronounced. In the opposite limit of a low symmetry $\mathbf{k}_{||}$ point all electron states are involved in $\pm m$ redistribution that makes the features of the nonmonotonic behavior less distinct.

To illustrate further the difference in the $\pm m$ redistribution at different $\mathbf{k}_{||}$ we plot in Fig. 11 the orbital polarizabilities of the electronic states. This quantity is calculated as follows: For a given state we divide the partial $3d$ orbital moment in the surface layer by the partial $3d$ charge in this layer. For the Γ point and FM0 structure [Fig. 11(a)] the orbital polarizability assumes, for many electron states, an integer value showing that the corresponding state has only one nonzero $3d$ m component. Different signs of the polarizability correspond to different m signs of these components. For the Γ point of the FM90 structure [Fig. 11(b)] and for the middle point of the ΓM interval for the both structures [Figs. 11(c) and 11(d)] the behavior of the polarizability is much less regular reflecting a much more complex process of the $\pm m$ redistribution.

It is worth remarking here that although the high symmetry of the Γ point leads to a most clear pattern of the nonmonotonic behavior in the considered occupation dependencies, this does not mean that the electronic states at the Γ point play a decisive role in the formation of the total MAE(N) and OMA(N) dependencies. The integral quantities MAE(N) and OMA(N) collect contributions of all $\mathbf{k}_{||}$ and their behavior is the result
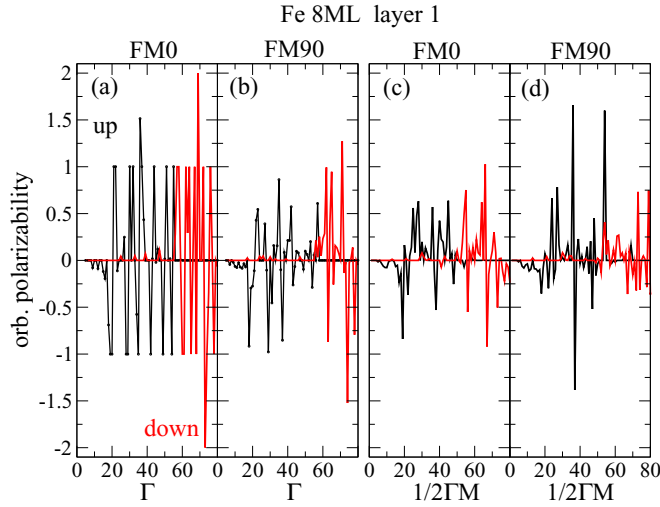
FIG. 11. (Color online) Orbital polarizability of the states in the surface layer of the 8-ML-thick film. Shown are the results for the Γ point and the center of the ΓM interval for both FM0 and FM90 structures. Black curves correspond to the spin-up contribution, red curves to the spin-down contribution.

of the averaging over the whole 2D BZ. As seen in Fig. 4 the N dependence of the OMA contribution of the Γ point [Fig. 4(b)] is principally different from the total OMA(N) dependence [Fig. 4(a)].

D. Systematic analysis of the $\mathbf{k}_{||}$-resolved contributions to MAE and OMA over the whole 2D BZ

In the analysis of the $\mathbf{k}_{||}$-resolved contributions to MAE and OMA it is important to take into account that the number of occupied states at a given $\mathbf{k}_{||}$ point can be different for the FM0 and FM90 structures. This results from the different influence of the SOC on the electronic states depending on the direction of the magnetization of the system. A relative shift of the energy levels caused by the SOC can lead at some $\mathbf{k}_{||}$ points to a lower number of the occupied states for FM0 structure compared to the FM90 structure and higher occupation of the FM0 electronic states at other $\mathbf{k}_{||}$ points. The contributions to MAE and OMA of a $\mathbf{k}_{||}$ point with different numbers of electrons ($\Delta n_k := n_k(\text{FM0}) - n_k(\text{FM90}) \neq 0$) for the FM0 and FM90 structures is very large since the input of extra electrons is not compensated at the same point. However, since the total number of electrons in the system is constant, an extra electron at a given $\mathbf{k}_{||}$ point in the FM0 structure must be compensated by an extra electron in the FM90 structure at another $\mathbf{k}_{||}$ point. Such a redistribution of electrons between $\mathbf{k}_{||}$ points complicates point-by-point analysis of the partial contributions to MAE and OMA. Fortunately, the calculations show that the part of the $\mathbf{k}_{||}$ points with different numbers of electrons and their contribution to the total anisotropies of the system are relatively small: The number of the $\mathbf{k}_{||}$ points with nonzero Δn_k is usually less than 10% of the total number of $\mathbf{k}_{||}$ in the mesh and the contribution of these points to the total MAE and OMA is usually below 15%. Therefore to get a qualitative insight into the $\mathbf{k}_{||}$ dependence of the contributions
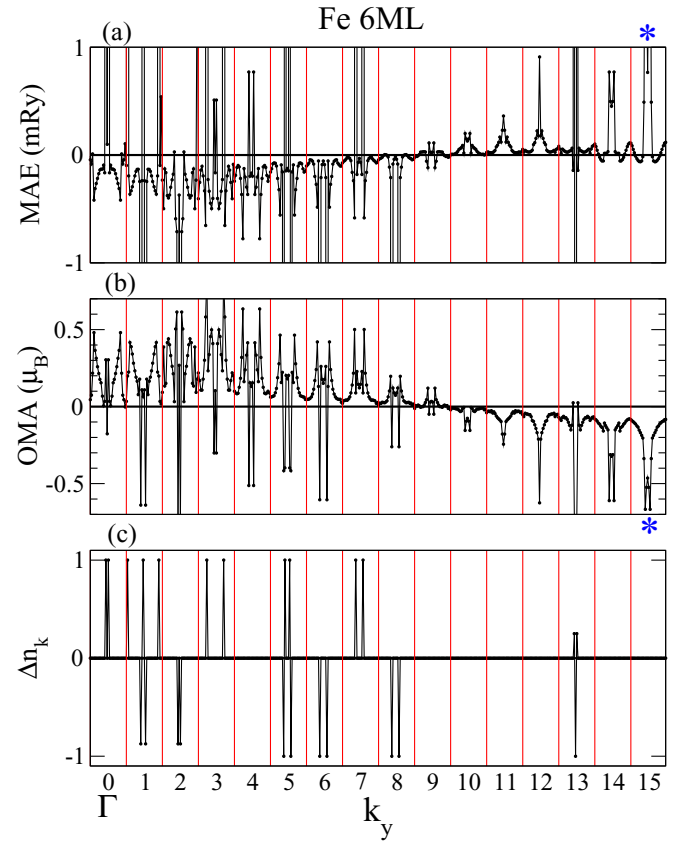

FIG. 12. (Color online) $\mathbf{k}_{||}$-resolved contributions to MAE (a) and OMA (b) for the 6-ML-thick Fe film; (c) shows Δn_k. The vertical red lines separate the 16 sub-blocks numbered at the bottom of the figure. Within each sub-block the k_x has a constant value of $k_x = i_{\text{sbl}}/30$ and k_y varies within the interval $(-0.5, 0.5)$ with constant mesh step of $\frac{1}{30}$. Here $i_{\text{sbl}} = 0, 1, ..., 15$ is the sub-block number. Blue asterisks in (a) and (b) mark the peaks whose origin in addressed in Fig. 13.

we can focus on the $\mathbf{k}_{||}$ points with an equal number of electrons ($\Delta n_k = 0$).

In Fig. 12 we present $\mathbf{k}$-resolved contributions to MAE and OMA for the 6-ML-thick film. The vertical red lines separate 16 sub-blocks numbered at the bottom of the figure. Within each sub-block the k_x has a constant value of $k_x = i_{\text{sbl}}/30$ and k_y varies within the interval $(-0.5, 0.5)$ with constant mesh step of $\frac{1}{30}$. Here $i_{\text{sbl}} = 0, 1, ..., 15$ is the sub-block number. The lowest panel shows Δn_k. The deviations from zero mark the $\mathbf{k}_{||}$ points with different occupations of FM0 and FM90 structures. Focusing on the points with $\Delta n_{\mathbf{k}_{||}} = 0$ we see again strong correlation between contributions to the MAE [Fig. 12(a)] and OMA [Fig. 12(b)]. Although the dependencies are not simply proportional to each other the positions of the peaks mostly coincide and the sign of the corresponding contributions is opposite for all strong features. Figure 12 shows that the contributions at the periphery of the BZ (large sub-block numbers i_{sbl}) differ by sign from the contributions of the sub-blocks with smaller i_{sbl}. The contribution of the Γ point corresponding to the center of the sub-block with $i_{\text{sbl}} = 0$ does not play any critical role in the formation of the anisotropy values.
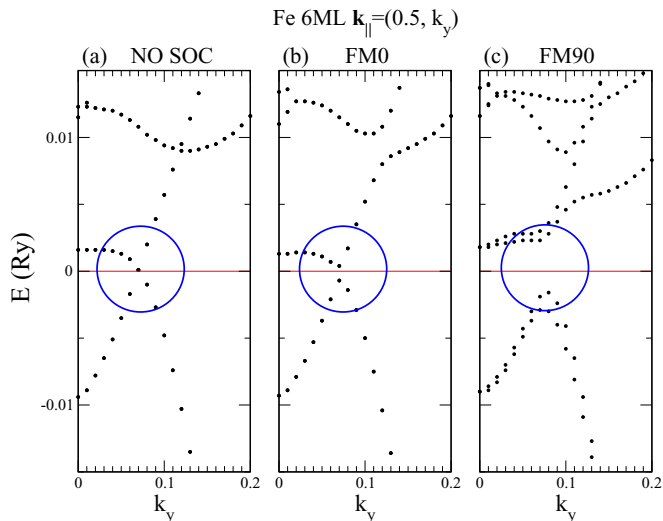
FIG. 13. (Color online) Fragment of the band structure of the 6-ML-thick film highlighting the formation of the peaks of MAE and OMA marked by blue asterisks in Fig. 12. (a) The energy bands of the ferromagnetic structure calculated without SOC. (b) The energy bands of the FM0 structure calculated with SOC. (c) The energy bands of the FM90 structure calculated with SOC.

The origin of the individual strong features in the $\mathbf{k}_{\|}$-resolved MAE and OMA can be found in the details of the response of the electronic states on the SOC for FM0 and FM90 structures. For example, the strong peaks in the 15th sub-block marked by the blue asterisks in Figs. 12(a) and 12(b) can be traced back to the features of the band structure of the film encircled in Fig. 13. The lower symmetry of the FM90 structure leads to the lifting of the band intersection Fig. 13 and results in a strong anisotropy effect.

In Fig. 14, a more compact presentation of the $\mathbf{k}_{\|}$-resolved data is given. Here we consider concentric squares in the 2D BZ with the center at the Γ point and add together the contributions of the $\mathbf{k}_{\|}$ points belonging to the perimeter of the same square. In the summation, we include only the points with $\Delta n_k = 0$. The figure presents the MAE and $-$OMA as functions of the size of the side of the square d. The analysis of Fig. 14 shows that, also in this type of presentation, the MAE and OMA
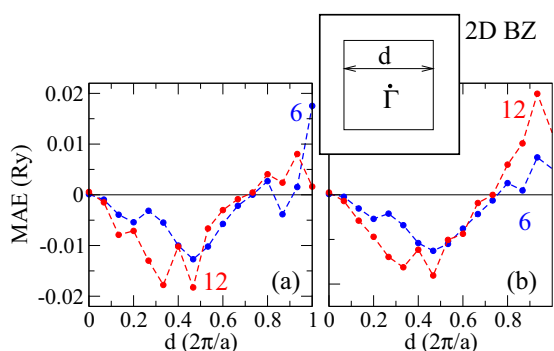

FIG. 14. (Color online) The contributions to MAE (a) and $-$OMA (b) from the concentric squares in the 2D BZ (the squares are shown in the insert). The results are presented for films with thicknesses $N = 6$ (blue) and $N = 12$ (red).
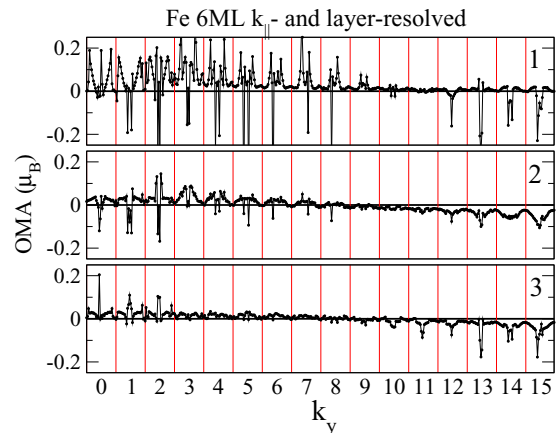

FIG. 15. (Color online) $\mathbf{k}_{\|}$- and layer-resolved contributions for the 6-ML thick film. The layer number is given in the left part of the figure. The first layer corresponds to the surface layer.

dependencies are similar. Both dependencies are negative in the main part of the interval of the d variation extended from 0 to 1 and change the sign at about $d = 0.8$. It is clearly seen that the Γ point and its nearest neighborhood (the region about $d = 0$) give a very small contribution to both quantities. Instead, large contributions come from the broad region of intermediate d values.

To discuss the layer dependence of the k-resolved OMA contributions we consider the layer-resolved OMA data. In Fig. 15, these data are presented for $N = 6$. In agreement with the layer-summed data [Fig. 12(b)] the sub-blocks of the $\mathbf{k}_{\|}$ points that are far from the Γ point (the sub-blocks with numbers 11–15) contribute with negative OMA. The sign of the contribution changes for the sub-block lying closer to the Γ point. The remarkable property of the layer-resolved data is that for the sub-blocks close to the zone boundary we do not observe the trend of decay of the contributions with increasing depth of the layer. This trend, however, is well seen for the sub-blocks closer to the Γ point (the sub-block numbers 0–8).

To demonstrate the general nature of the difference in the character of layer dependencies in different parts of the BZ we show in Fig. 16 the layer-resolved data for the thickest studied film with $N = 24$. Also here the negative contributions of the periphery sub-blocks do not decay with increasing depth of the layer but, instead, remain rather constant. On the contrary, for the sub-blocks close to the Γ point the OMA contributions clearly decrease with increasing depth and are rather small for the third and fourth layer. Then they increase again not reaching, however, the large value obtained for the surface layer. Thus we see that the spatial distribution of the $3d$ QWS contributing to the MAE and OMA is different in different parts of the 2D BZ.

The experimental data always reflect the result of different types of effective averaging. Above, we already discussed the averaging over $\mathbf{k}_{\|}$. Another origin of averaging is varying thickness of each film. Indeed, the films are never ideally flat and, therefore, thickness is not a uniform characteristic of the real film. Even assuming an ideal substrate, it is impossible to fabricate an ideally flat film. The substrate is not, however, ideally flat. In the experimental papers we discuss the stepped
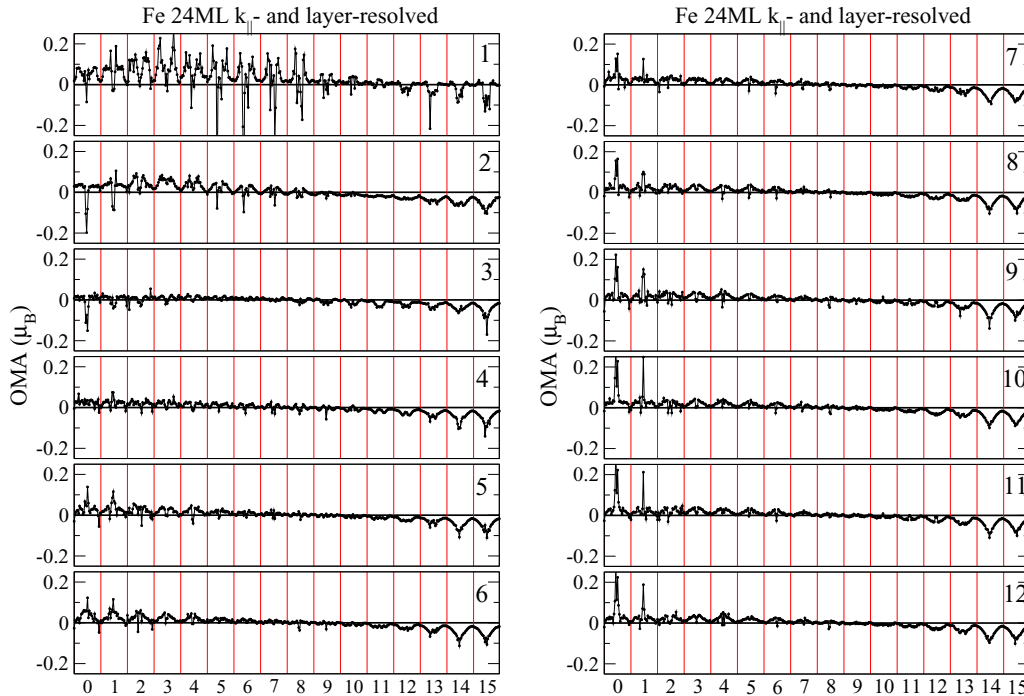
FIG. 16. (Color online) Similar to Fig. 15 but for the film of the 24-ML thickness.

substrates were selected purposely. The nonideality of the films diminishes the symmetry of the system and leads to further increase of the number of electronic states involved in intense $\pm m$ redistribution. In the given paper we restrict the calculations to the ideally flat films that gives an insight into the process of the formation of the correlating oscillating character of MAE and OMA and provides the basis for the studies of more complex situations.

IV. NONCOLLINEAR MAGNETIC STRUCTURES

In this section we briefly address two experimental observations which did not find an explanation within the simplified treatment of the electronic structure used in the experimental papers [18,21,22].

The first observation is a strong spin mixing of the initial electronic states of the photoemission process reported in Ref. [22]. The states lie about 0.2 eV below the Fermi level and are ascribed by the authors to the Γ point of the 2D BZ. The nature of the states is attempted to be understood in terms of the electronic structure of the bulk bcc Fe at the ΓH symmetry line in the 3D BZ. The measured spin polarization is about 45%. The authors conclude that "the probed initial state is a mixture of majority and minority states." The explanation of the origin of the spin mixing was not found since in the band structure at the ΓH interval in the bulk BZ there is no close in energy spin-up and spin-down states that can hybridize strongly under the influence of the SOC. The question about the origin of the strong spin mixing was left open.

We see a number of contributions to the observed spin mixing. First, as we already pointed out the reference to the bulk band structure in the study of the properties of thin films can be very misleading. The explanation should be looked for in the properties of the systems studied in the

experiment. The films studied experimentally are not ideally flat and contain steps. This means that the symmetry of the real film is decreased compared to the symmetry of the ideal films studied in the present work. Even in-plane translational symmetry is disturbed by the steps. As discussed above, the lowering of symmetry leads to the involvement of more states in the hybridization caused by the SOC. For instance, in an ideally flat film the states with different $\mathbf{k}_{||}$ do not hybridize and the influence of the SOC on the states can be considered for each $\mathbf{k}_{||}$ separately. The loss of the in-plane periodicity destroys $\mathbf{k}_{||}$ as a good quantum number and leads to the spin mixing of the states that in a flat film belong to different $\mathbf{k}_{||}$. This enhanced spin mixing can be an important contribution to the observed strong spin mixing. Since in the present work we do not study the stepped films this suggestion has here the status of hypothesis.

Second, the measurements are performed for nonzero temperature ($T = 300$ K) and, therefore, the thermal disordering of the atomic moments should be taken into account. The noncollinearity of the atomic moments, similar to the SOC, leads inevitably to the spin mixing of the electronic states. The spin mixing increases with increasing angles between atomic moments. More generally, any deviation of the atomic moments from the direction of the net magnetization leads to the spin mixing with respect to the spin-quantization axis parallel to the direction of the net magnetization. In the experiment, the spin mixing is measured with respect to the direction of net magnetization.

We argue that the spin disordering is also important for the understanding of the thermal decay of the oscillating behavior of the MAE(N). This decay takes place at the temperatures considerably below the Curie temperature. As discussed in the introduction, the authors of the experimental works [18,21] draw the conclusion that the disappearance of

the oscillations cannot be a "thermal" effect since the exchange splitting between spin-up and spin-down states is much larger than the temperature at which the oscillations disappear. This argument is, however, valid only within the Stoner theory neglecting transverse fluctuations of the atomic spin moments. The transverse spin fluctuations are less energetic than single-electron Stoner excitations and are responsible for the thermal decrease of the magnetization.

In Fig. 3(c) we present the results of the calculation of the MAE and OMA for the noncollinear spin configuration of the type shown in the insert in Fig. 7. Figure 7 shows that the calculated electronic energies at the Γ point of the noncollinear structure are very different from the spectra for the ferromagnetic configuration of the same film. Although the correlation between MAE(N) and OMA(N) is preserved also for the noncollinear spin structure [Fig. 3(c)] there is considerable change of the oscillating behavior compared to the collinear ferromagnetic structure [Fig. 3(b)]. For instance, very strong drop of the MAE and $-$OMA at $N = 7$ compared to $N = 6$, present for the collinear structure, is absent for the NC30 structure; in the NC30 structure there is no maximum at $N = 13$; the minimum at $N = 19$ is replaced by maximum and the maximum at $N = 20$ is replaced by minimum.

The physical quantities at nonzero temperatures are the result of the statistical mechanics averaging over configurations with various levels of noncollinearity. The larger is the temperature the larger is the contribution of the noncollinear configurations. Our calculations demonstrate strong dependence of the oscillating behavior on the magnetic structure. The dependence of the features of the nonmonotonic dependence of MAE and OMA on the leads to the smoothing of these features as the result of the averaging over spin configurations that is supplementary to the averaging over $\mathbf{k}_{||}$ points discussed above.

V. CONCLUSION

We report the first-principles study of the correlated behavior of the magnetic anisotropy energy and orbital moment anisotropy as the functions of the thickness N of the Fe film. The work is motivated by recent experimental studies combining photoemission, x-ray magnetic circular dichroism, and magnetic anisotropy measurements. In agreement with experiment, the correlated oscillations of MAE(N) and OMA(N) are obtained that have their origin in the formation of the $3d$ quantum well states confined in the films. The main contribution to the oscillation amplitude comes from the surface layer. This is an interesting feature of the phenomenon consisting in the peculiar dependence of the physical quantities on the thickness of the film.

The key feature behind both MAE and OMA is the $\pm m$ polarization of the electron states by the SOC. This feature provides the understanding of the correlation in the properties of MAE and OMA. The $\pm m$ polarizability varies from $\mathbf{k}_{||}$ point to $\mathbf{k}_{||}$ point making necessary a careful analysis of the partial $\mathbf{k}_{||}$ contributions and their summation.

We demonstrate that the band structure of the bulk Fe does not reflect adequately the properties of the $3d$ QWS in thin films and, therefore, does not provide the basis for understanding of the oscillations of MAE(N) and OMA(N). A detailed point-by-point analysis in the 2D Brillouin zone (BZ) of the film shows that the contribution of the Γ point, contrary to a rather common expectation, does not play an important role in the formation of the oscillations. Instead, the most important contributions come from a broad region of the 2D BZ distant from the center of the BZ.

Combining symmetry arguments and direct calculations we show that orbital moments of the electronic states possess nonzero transverse components orthogonal to the direction of the spin magnetization. The account for this feature is crucial in the point-by-point analysis of the OMA. On the basis of the calculations for noncollinear spin configurations we suggest interpretations of two interesting experimental findings: fast temperature decay of the oscillation amplitude in MAE(N) and unexpectedly strong spin mixing of the initial states of the photoemission process.

Our calculations in agreement with earlier calculations [17] for Co films did not result in the decay of the oscillation amplitude with increasing film thickness. Since the experimental data apparently show such a decay for the interval of film thicknesses studied in the given paper it remains an important theoretical task to understand and describe this decay. It can be many reasons for the decay of the oscillation amplitude in the experiment. An important factor is the imperfectness of the films grown on a stepped substrate that leads to varying thickness for a given sample. Another possibility is a finite quantum mechanical coherence of the electronic states that can become comparable or less than the film thickness. The many-body effects can be important leading to an effective shift and broadening of the electronic states. This interesting problem is beyond the scope of the given paper and must be the topic of separate studies.

The extension of the first-principles calculations within the framework of the density functional theory on the nonideal films grown on stepped substrates is desirable.

[1] M. Cinal, D. M. Edwards, and J. Mathon, Phys. Rev. B **50**, 3754 (1994).

[2] W. Weber, A. Bischof, R. Allenspach, Ch. Würsch, C. H. Back, and D. Pescia, Phys. Rev. Lett. **76**, 3424 (1996).

[3] S. S. P. Parkin, N. More, and K. P. Roche, Phys. Rev. Lett. **64**, 2304 (1990).

[4] J. Unguris, R. J. Celotta, and D. T. Pierce, Phys. Rev. Lett. **67**, 140 (1991).

[5] P. Bruno, Phys. Rev. B **52**, 411 (1995).

[6] J. E. Ortega and F. J. Himpsel, Phys. Rev. Lett. **69**, 844 (1992).

[7] M. Milun, P. Pervan, B. Gumhalter, and D. P. Woodruff, Phys. Rev. B **59**, 5170 (1999).

[8] Shinji Yuasa, Taro Nagahama, Takateru Kawakami, Koji Ando, and Yoshishige Suzuki, J. Phys. D **35**, 2427 (2002).

[9] Y. Suzuki, T. Katayama, P. Bruno, S. Yuasa, and E. Tamura, Phys. Rev. Lett. **80**, 5200 (1998).

[10] L. Aballe, A. Barinov, A. Locatelli, S. Heun, and M. Kiskinova, Phys. Rev. Lett. **93**, 196103 (2004).

[11] N. V. Smith, Phys. Rev. B **32**, 3549 (1985).

[12] N. V. Smith, N. B. Brookes, Y. Chang, and P. D. Johnson, Phys. Rev. B **49**, 332 (1994).

[13] J. E. Ortega, F. J. Himpsel, G. J. Mankey, and R. F. Willis, Phys. Rev. B **47**, 1540 (1993).

[14] D.-A. Luh, J. J. Paggel, T. Miller, and T.-C. Chiang, Phys. Rev. Lett. **84**, 3410 (2000).

[15] M. Cinal, J. Phys.: Condens. Matter **15**, 29 (2003).

[16] G. Y. Guo, J. Phys.: Condens. Matter **11**, 4329 (1999).

[17] L. Szunyogh, B. Ujfalussy, C. Blaas, U. Pustogowa, C. Sommers, and P. Weinberger, Phys. Rev. B **56**, 14036 (1997).

[18] J. Li, M. Przybylski, F. Yildiz, X. D. Ma, and Y. Z. Wu, Phys. Rev. Lett. **102**, 207206 (2009).

[19] J. Li, M. Przybylski, Y. He, and Y. Z. Wu, Phys. Rev. B **82**, 214406 (2010).

[20] U. Bauer and M. Przybylski, Phys. Rev. B **81**, 134428 (2010).

[21] J. Li, G. Chen, Y. Z. Wu, E. Rotenberg, and M. Przybylski, IEEE Trans. Magn. **47**, 1603 (2011).

[22] M. Dabrowski, T. R. F. Peixoto, M. Pazgan, A. Winkelmann, M. Cinal, T. Nakagawa, Y. Takagi, T. Yokoyama, F. Bisio, U. Bauer, F. Yildiz, M. Przybylski, and J. Kirschner, Phys. Rev. Lett. **113**, 067203 (2014).

[23] P. Bruno, Phys. Rev. B **39**, 865 (1989).

[24] L. M. Sandratskii, J. Phys.: Condens. Matter **26**, 426001 (2014).

[25] I. Turek, J. Kudrnovsky, and K. Carva, J. Supercond. Nov. Magn. **36**, 1581 (2013).

[26] L. M. Sandratskii, Adv. Phys. **47**, 91 (1998).

[27] G. Y. Guo, W. M. Temmerman, and H. Ebert, J. Phys.: Condens. Matter **3**, 8205 (1991).

[28] Z. Q. Qiu, J. Pearson, and S. D. Bader, Phys. Rev. Lett. **70**, 1006 (1993).

[29] A. Hahlin, C. Andersson, J. H. Dunn, B. Sanyal, O. Karis, and D. Arvanitis, Phys. Rev. B **73**, 134423 (2006).